J Mater Sci (2007) 42:1517–1528
DOI 10.1007/s10853-006-0628-0

Evolution of microstructure and microtexture in fcc metals during high-pressure torsion

A. P. Zhilyaev · T. R. McNelley · T. G. Langdon

Received: 30 May 2006 / Accepted: 27 June 2006 / Published online: 21 December 2006

Abstract Pure nickel and commercially pure (CP) aluminium were selected as model fcc materials for a detailed investigation of the experimental parameters influencing grain refinement and evolution of microstructure and microtexture during processing by high-pressure torsion (HPT). Samples were examined after HPT using microhardness measurements, transmission electron microscopy and orientation imaging microscopy. Processing by HPT produces a grain size of ~170 nm in pure Ni and ~1 μm in CP aluminium. It is shown that homogeneous and equiaxed microstructures can be attained throughout the samples of nickel when using applied pressures of at least ~6 GPa after 5 whole revolution. In CP aluminium, a homogeneous and equiaxed microstructure was achieved after 2 whole revolutions under an applied pressure of 1 GPa. For these conditions, the distributions of grain boundary misorientations are similar in the centre and at the periphery of the samples. It is shown that simple shear texture develops in fcc metals subjected to high-pressure torsion. Some grain growth was detected at the periphery of the Al disk after 8 revolutions. The factors influencing the development of homogeneous microstructures in processing by HPT are discussed.

A. P. Zhilyaev
Department of Physical Metallurgy, Centro National de Investigaciones Metallúrgicas, CSIS 28040, Madrid, Spain

T. R. McNelley
Department of Mechanical and Astronautical Engineering, Naval Postgraduate School, Monterey, CA 93943-5100, USA

T. G. Langdon
Departments of Aerospace & Mechanical Engineering and Materials Science, University of Southern California, Los Angeles, CA 90089-1453, USA

A. P. Zhilyaev (✉)
Institute for Superplasticity Metals Problems, RAS, 450001, Ufa, Russia
e-mail: zhilyaev@cenim.csic.es

Introduction

Two different procedures are generally used in processing through the application of Severe Plastic Deformation (SPD). The first, known as Equal-Channel Angular Pressing (ECAP), involves pressing a bar or rod through a die within a channel bent into an L-shaped configuration [1]. The second, known as High-Pressure Torsion (HPT), involves subjecting a sample, in the form of a thin disk, to a high pressure and concurrent torsional straining [2]. Early experimental evidence suggested that HPT may be more effective than ECAP in producing exceptionally small grain sizes: for example, experiments on an Al-3% Mg solid solution alloy gave a grain size of ~90 nm when processing using HPT at room temperature [3] whereas a similar alloy processed by ECAP at room temperature yielded a grain size of ~270 nm [4]. The greater grain refinement achieved in HPT has been confirmed recently in two different ways. First, by processing the same alloy using both procedures where there are reports of grain sizes of ~150 nm after HPT and ~600 nm after ECAP in an Al-2% Fe alloy [5] and ~170 nm after HPT and ~350 nm after ECAP in high purity Ni [6]. Second, by subjecting samples of pure Ti to HPT after processing by ECAP where it was

demonstrated that there was an additional reduction in the grain size from ~300 nm to ~200 nm [7]. In addition, whereas the grain sizes attained in ECAP are generally in the submicrometer range of ~100–1,000 nm, numerous reports are now available documenting grain sizes of <100 nm in materials processed by HPT: for example, nanometer grains sizes have been reported in various Al alloys [8–10], a Cu nanocomposite [11], various Ni alloys [12, 13], Ni_3Al [14–16], Ti-6% Al-4% V [17] and various steels [10, 18–22].

To date, three different types of HPT dies have been employed in order to obtain HPT disks, namely unconstrained [6, 23] and two forms of constrained [24–26]. A detailed description of the principles of these HPT procedures is given in Section 2. In a detailed investigation of pure nickel [23], it was shown that microstructural evolution begins at the outer edges of the disks used in HPT and the evolution spreads gradually to the centres of the disks with increasing imposed strain. These observations suggest that the microstructure becomes reasonably homogeneous at high total strains although it should be noted this homogeneity is inferred indirectly from the consistency in microhardness measurements taken across the specimen diameters and there may remain some microstructural inhomogeneities when detailed observations are made using transmission electron microscopy (TEM). Similar conclusions may be drawn from studies performed on CP aluminium [27] and an Al-alloy [25] subjected to constrained HPT and a NiTi alloy [28]. By contrast, a very recent report described the development of inhomogeneities in an austenitic steel when microhardness measurements were taken after HPT processing although the microhardness measurements were not supported by corresponding observations using TEM [24].

The present investigation was initiated to review existing results and to obtain a better understanding of the evolution of microstructure and microtexture during HPT. Some possible explanations of this apparent discrepancy are suggested and a simplified model for microstructural evolution during HPT testing is discussed.

Principles of HPT and estimating the strain

In processing by HPT, the samples are in the form of thin disks and they are placed in the HPT facility between upper and lower anvils, subjected to a very high pressure and then strained in torsion where the straining is usually achieved by rotating the lower anvil. Three distinct types of HPT processing are illustrated schematically in Fig. 1: these types are termed (a) unconstrained and (b, c) constrained HPT, respectively.

In constrained HPT, the disk is machined to fit into a cavity in the lower anvil (or both) and the load is applied so that, in principle at least, there is no outward flow of material under the application of a high load. Constrained HPT is therefore conducted in the presence of a back-pressure. In practice, however, it is difficult to achieve an idealized constrained condition and there is generally at least some limited flow between the upper and lower anvils. In unconstrained HPT, the specimen is free to flow outwards under the applied pressure and little or no back-pressure is introduced into the system.

Both constrained and unconstrained HPT have been used in prior experiments. Thus, an earlier investigation of pure Ni was conducted using unconstrained HPT [23, 29] whereas the experiments on austenitic steel used constrained HPT although it was noted there was some limited outward flow of material between the two anvils on application of the load [24]. In the present work, the HPT processing was conducted using an unconstrained HPT facility for the nickel specimens and a constrained facility for CP aluminium.

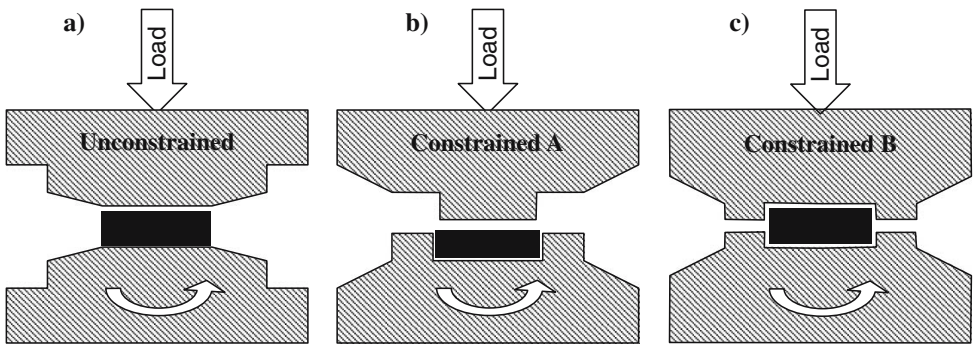

Fig. 1 Principles of HPT for (**a**) unconstrained and (**b**, **c**) two types of constrained conditions

The sample, in the form of a disk, is located between two anvils where it is subjected to a compressive applied pressure, P, of several GPa at room temperature and simultaneously to a torsional strain which is imposed through rotation of the lower support. Surface frictional forces therefore deform the disk by shear so that deformation proceeds under a quasi-hydrostatic pressure. For an infinitely small rotation, $d\theta$, and displacement, dl, it follows that $dl = r\,d\theta$ where r is the radius of the disk and the incremental shear strain, $d\gamma$, is given by

$$d\gamma = \frac{dl}{h} = \frac{rd\theta}{h}, \tag{1}$$

where h is the disk thickness.

Assuming that the thickness of the disk is independent of the rotation angle, θ, formal integration can be used so that, noting $\theta = 2\pi N$, it follows that

$$\gamma = \frac{2\pi N \cdot r}{h} \tag{2}$$

where N is a number of revolutions.

An equivalent strain has been calculated in many publications using the von Mises relationship:

$$\varepsilon = \gamma \Big/ \sqrt{3}. \tag{3}$$

The use of Eq. (3) is correct only in the case of a small imposed shear strain. For a large shear strain, $\gamma \geq 0.8$, the correct equation for the equivalent strain gives [30]:

$$\varepsilon = \left(2\Big/\sqrt{3}\right) \ln\left[\left(1+\gamma^2/4\right)^{1/2} + \gamma/2\right] \tag{4}$$

A similar relationship has also been developed which incorporates the decrease in thickness of the disk as a consequence of the applied pressure, P. For this condition, the true strain is given by [31]

$$\varepsilon = \ln\left[1 + \left(\frac{\theta \cdot r}{h}\right)^2\right]^{1/2} + \ln\frac{h_0}{h}, \tag{5}$$

where h_0 and h are initial and final thickness, respectively. In practice, Eq. (5) can be further simplified because, since $(\theta \cdot r/h) >> 1$, it follows that [32]

$$\varepsilon = \ln\left[1 + \left(\frac{\theta \cdot r}{h}\right)\right] + \ln\frac{h_0}{h} \tag{6}$$

Thus, Eqs. (3) to (6) provide relationships that may be used to estimate the total strains within disks subjected to HPT. Figure 2 shows accumulated strain calculated using Eqs. (2) and (4) for the conditions where r = 10, 5, 1 or 0.1 mm and h = 0.1 mm as a function of the number of whole revolutions. It can be seen that a quasi-saturation occurs already at N = 2 revolutions and the difference in accumulated strain is not drastically large for points at the periphery (r = 10 mm) and near the centre (r = 1 mm). Even for r = 0.1 mm, the accumulated strain after 5 whole revolutions equals 4 and this is only 2.5 times lower that at the periphery. If it is assumed that there is no straining at r = 0 mm, there is a low probability of detecting the centre with a precision better than 0.1 mm. Also, it is important to note that usually the TEM foils are 3 mm in diameter and obtaining a transparent area by jet electro-polishing is an uncontrollable and essentially random operation. Therefore, in practical terms at least, it is not feasible to accurately detect and examine the centre of the HPT disk. Based on the uncertainties in calculating strain, it is reasonable to agree with an earlier suggestion that the straining introduced in HPT is most realistically expressed by simply specifying the number of revolutions imposed on the sample.

Experimental material and procedures

High purity nickel (99.99%) was selected for use in this investigation. The nickel samples were annealed for 6 h at 973 K prior to HPT to give a relaxed microstructure with an initial grain size of ~100 μm and an initial hardness of ~1.4 GPa. In practice, preliminary

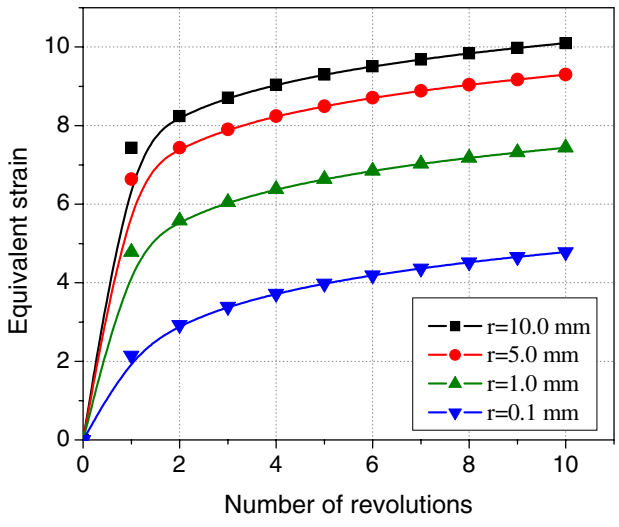

Fig. 2 Equivalent strain as a function of number revolutions and distance from the centre of HPT disks calculated using eqs. (2) and (4)

studies have shown that the final microstructures produced by HPT are essentially independent of the initial grain size within the range of ~1–100 μm. High-pressure torsion (unconstrained) was applied at room temperature. Specifically, samples were prepared in the form of small disks with diameters of ~10 mm and thicknesses of ~0.3 mm and they were inserted into an apparatus similar to that shown in Fig. 1(a). The influence of the applied pressure was evaluated by subjecting samples to a total of 5 complete revolutions under separate imposed pressures of 1, 3, 6 and 9 GPa. The influence of the accumulated strain was evaluated by maintaining a constant pressure of 6 GPa and torsionally straining separate samples through totals of 0.5, 1, 3, 5 and 7 revolutions. Following HPT, precise microhardness measurements were taken on the surfaces of the nickel samples along diameters positioned at rotational increments of 45° about the central point of each disk. These measurements were taken in incremental steps along every diameter at positions ~1.25 mm apart and at every point the average microhardness was determined from four separate measurements clustered around the selected position. These locations are illustrated schematically in Fig. 3 where the insert on the right shows the selected position, marked by a star, and the four measurement points located around and in the immediate vicinity of the point. Nickel samples were examined by transmission electron microscopy (TEM) after HPT by cutting small pieces from either the centres or the peripheral areas of the disks in the immediate vicinity of the edge: the two positions selected for the TEM foils are also indicated in Fig. 3.

Aluminium of commercial purity (99.7%) was also used in this study. The material was annealed for one hour at 600 °C in air and then furnace cooled to give an initial grain size of ~0.2–0.5 mm. Disks were cut having diameters and thicknesses of 10 and 1 mm, respectively, and these disks were subjected to HPT under constrained conditions using a compressive pressure of 1 GPa. As discussed earlier, it is difficult to precisely specify the imposed strain in HPT and thus, following an earlier suggestion [23], the strain is specified in terms of the total number of whole revolutions applied to the disk, N. In the present experiments, aluminium disks were strained through 1, 2, 4 and 8 revolutions. Following HPT, the samples were ground, mechanically polished and then electro-polished. Microhardness measurements were taken using a Micromet 2,000 facility, with 5 separate measurements taken for each point using a load of 50 g and a loading time of 5 s. Foils were prepared for TEM from 3 mm disks cut from either the central region or the periphery of the HPT disks. The initial microstructure was also examined using optical microscopy.

Microtexture and grain boundary statistics in HPT nickel were recorded using a Philips XL-30 FEG scanning electron microscope with a TSL orientation imaging system [33]. The HPT aluminium was studied using SEM (TOPCON) with tungsten filament and TSL-OIM 4 system. The nickel OIM data were reanalysed using the same clean-up procedure as for the Al specimens and described in detail below. It should be noted that the clean-up procedure can significantly influence the measured microstructural parameters and this explains the present data for nickel is slightly different from the data published in an earlier paper [6]. The present clean-up procedure was performed in an OIM-TSL analyser including: (i) Grain Dilation (GD) with grain tolerance angle (GTA) equals 2° and minimum grain size of 2 pixels; (ii) Grain Confidence Index Standardization with a similar GTA = 2° and a similar value of the minimum grain size; (iii) Neighbor Orientation Correlation with a minimum confidence index of 0.05. The total number of modified points was not higher than 10% of the total points measured in the experiments.

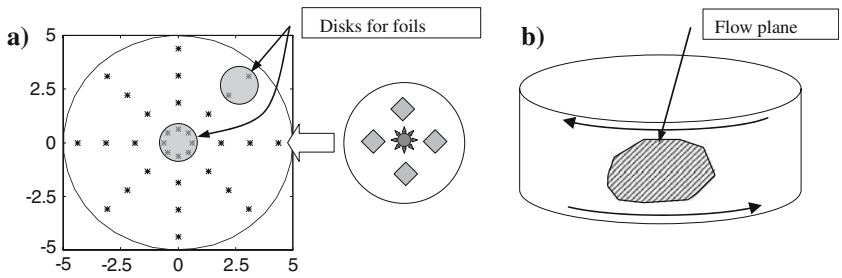

Fig. 3 (**a**) Schematic illustration of the procedure used for taking the microhardness measurements and for cutting disks for subsequent TEM observations: the insert on the right shows that four separate hardness measurements were recorded around each selected point; (**b**) flow plane of simple shear during HPT torsioning

Experimental results

Microhardness distribution and microstructure in nickel

A detailed description of microhardness measurements and TEM microstructure can be found elsewhere [23] where the influence of the applied pressure on the microhardness profiles for disks subjected to 5 whole revolutions under applied pressures of 1, 3, 6 and 9 GPa was reported. The influence of the magnitude of the torsional strain was also studied where the applied pressure was maintained constant at 6 GPa and the disks were subjected to 0.5, 1, 3 and 7 whole revolutions. All data were plotted in the form of three-dimensional meshes and the local hardness values within these meshes are then projected onto the lower plane and represented as hardness contours where separate hardness values are distinguished using contours of different colours: the precise significance of these coloured contours is indicated by the numbers, representing the hardness in GPa, associated with each contour line.

In the present paper, selected data are presented for illustration purpose. Fig. 4 shows a 3D mesh of the local hardness value and the corresponding TEM microstructure for the central region and for the periphery. Inspection shows that all measured values of the local microhardness are larger than for the unprocessed nickel where initially there was a hardness of ~1.4 GPa. It is also apparent that the microhardness values are generally non-uniform across the diameters of the samples and there are lower hardness values in the centres of the disk. The asymmetry visible at some of the applied pressures in Fig. 4 is attributed to the development of non-homogeneity of hardening during deformation in HPT since it is apparent that the evolution of hardness with increasing pressure is essentially a non-homogeneous process. At the pressure of 3 GPa, the microhardness increases primarily at the outer edge of the disk as anticipated from the higher strains evident in Fig. 4. However, this non-uniformity is gradually removed as the pressure increases and there is a reasonably homogeneous distribution of hardness values all lying at a level of >3 GPa. This is evident from Fig. 5 where a 3D mesh plot of Hv is presented with the related OIM colour coded maps. The microhardness value is notably higher than the initial one and apparently more homogeneous by comparison with the data in Fig. 4. The increase in the average value of the microhardness with increasing applied pressure appears to be due to the development of higher microhardness values around the periphery of the disk and the subsequent sweeping of these areas of higher hardness across the disk.

Foils were examined by TEM for all of the experimental conditions used to construct the three-dimensional meshes in Fig. 4. Representative examples are shown in Fig. 4 (b, c) where Fig. 4b corresponds to the centres of the disks and Fig. 4c corresponds to the peripheries of the disks (as defined in Fig. 3) and bright-field images are illustrated for the condition of the applied pressure of 3 GPa and for $N = 5$ whole revolutions; also shown as inserts in Fig. 4 (b, c) are the SAED patterns for each condition. Inspection of these microstructures reveals important characteristics. First, the mean grain size at the centre of the disk tends to be larger than at the periphery. At $P = 3$ GPa, there is little difference in grain size between the centre and the periphery but there is a significant difference in the grain morphology because the grains tend to be reasonably equiaxed at the periphery but in the centre they are elongated and more similar to a conventional rolling microstructure. Measurements under these conditions gave an equiaxed grain size of ~0.2 μm at the periphery but there were elongated grains in the centre having dimensions of ~0.2×0.7 μm^2.

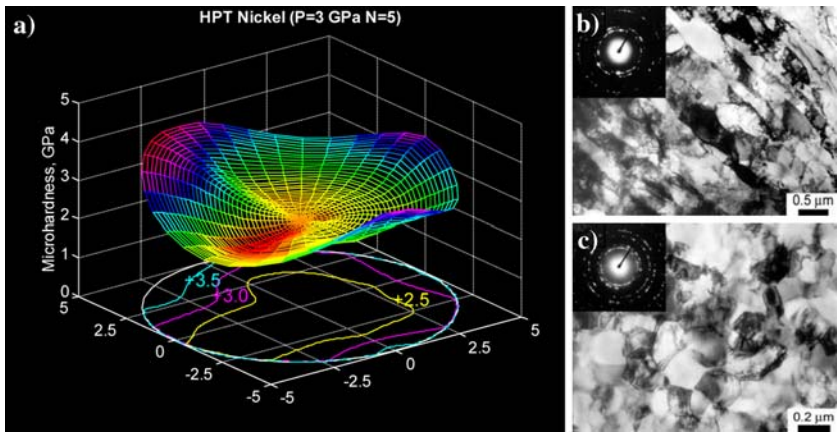

Fig. 4 Three-dimensional representations of the local microhardness for disks subjected to 5 whole revolutions under applied pressures of 3 GPa (**a**): TEM microstructure together with the associated SAED patterns: (**b**) corresponds to the centres of the disks; (**c**) to the peripheries of the disks

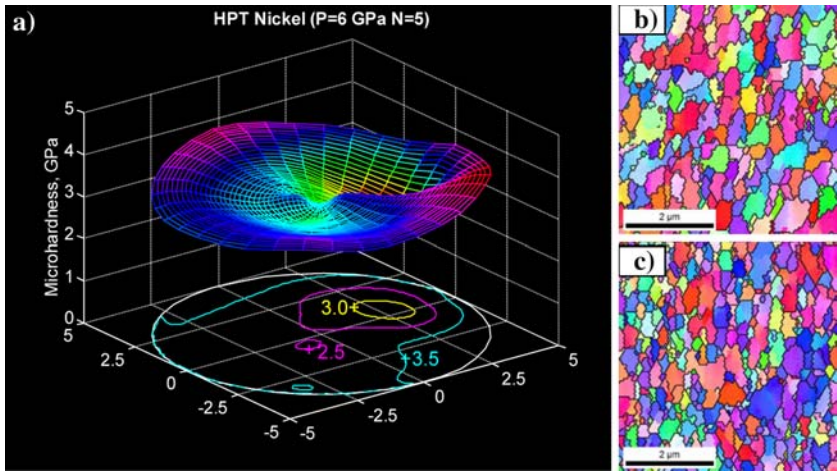

Fig. 5 Three-dimensional representations of the local microhardness for disks subjected to 5 whole revolutions under applied pressures of 6 GPa (**a**); OIM colour map: (**b**) corresponds to the centres of the disks; (**c**) to the peripheries of the disks

A similar tendency in microstructure was detected in an OIM study of the central region and periphery of the HPT nickel (Fig. 5) subjected to 5 whole revolutions under an applied pressure of 6 GPa. The mean grain size in the centre (Fig. 5b) is about 0.2–0.5 μm and this is slightly larger than the value of ~0.2 μm at the periphery (Fig. 5c). The grains tend to be reasonably equiaxed both at the periphery and in the centre.

Microhardness profile and TEM/OIM structure in commercially pure aluminium

The microhardness data [27] recorded for the HPT samples are depicted in Fig. 6 for conditions where the external pressure was $P = 1$ GPa. The lower dashed line indicates a microhardness of $Hv \approx 210$ MPa recorded for the material in the initial annealed condition, where this value is close to the value of ~150 MPa generally reported for pure aluminium. The lower set of experimental points, lying in the vicinity of $Hv \approx 320$ MPa, represent the measured hardness across the disk immediately after application of the load but without any torsional straining so that $N = 0$. For the situation where $N = 1$, there is a sharp minimum in Hv in the centre of the disk with a value close to the microhardness of the compressed disk but at the outer edges of the disk the microhardness reaches a saturation level in the vicinity of $Hv \approx 600$ MPa. It is apparent that the values of Hv in the central region increase with the number of whole revolutions and thus with the total imposed strain. For the samples subjected to 4 and 8 whole revolutions, there is reasonable homogeneity across the diameters with an average value of $Hv \approx 610$ MPa.

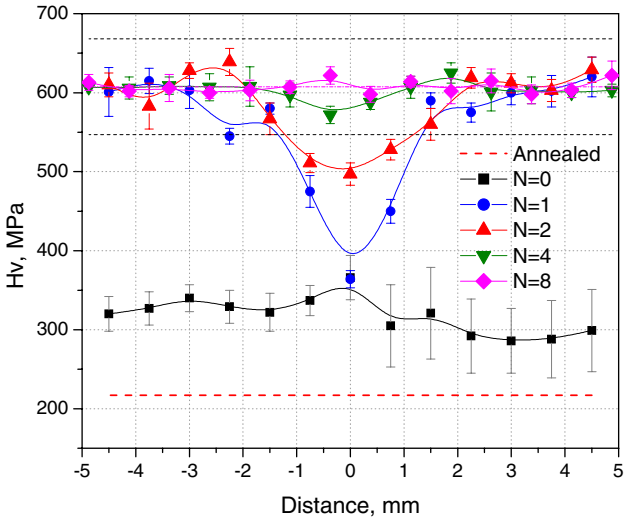

Fig. 6 Microhardness distributions across the diameters of aluminium disks subjected to a pressure of $P = 1$ GPa and up to 8 whole numbers of revolutions: the lower broken line shows the initial annealed condition

The datum points shown in Fig. 6 include the error bars calculated at the 95% confidence level. In practice, however, there tends to be some scatter between different operators in taking microhardness measurements and it is probably more realistic to assume a potential maximum error of ±10%: the two upper dotted lines correspond to this error range. It is concluded from Fig. 6 that, at least at the macroscopic level, there is reasonable homogeneity across the disks at values of N equal to or greater than 4 revolutions.

Figure 7a exhibits the microstructure of the initial condition using optical microscopy. Fig. 7b shows TEM micrographs of the structure after compression (at 1 GPa) without rotation. The TEM microstructures of the central region and near the periphery of the disks after 2 (Fig. 7c, d) and 8 (Fig. 7e, f) whole revolutions are also presented. Careful inspection shows that the grain size after 2 whole revolutions is

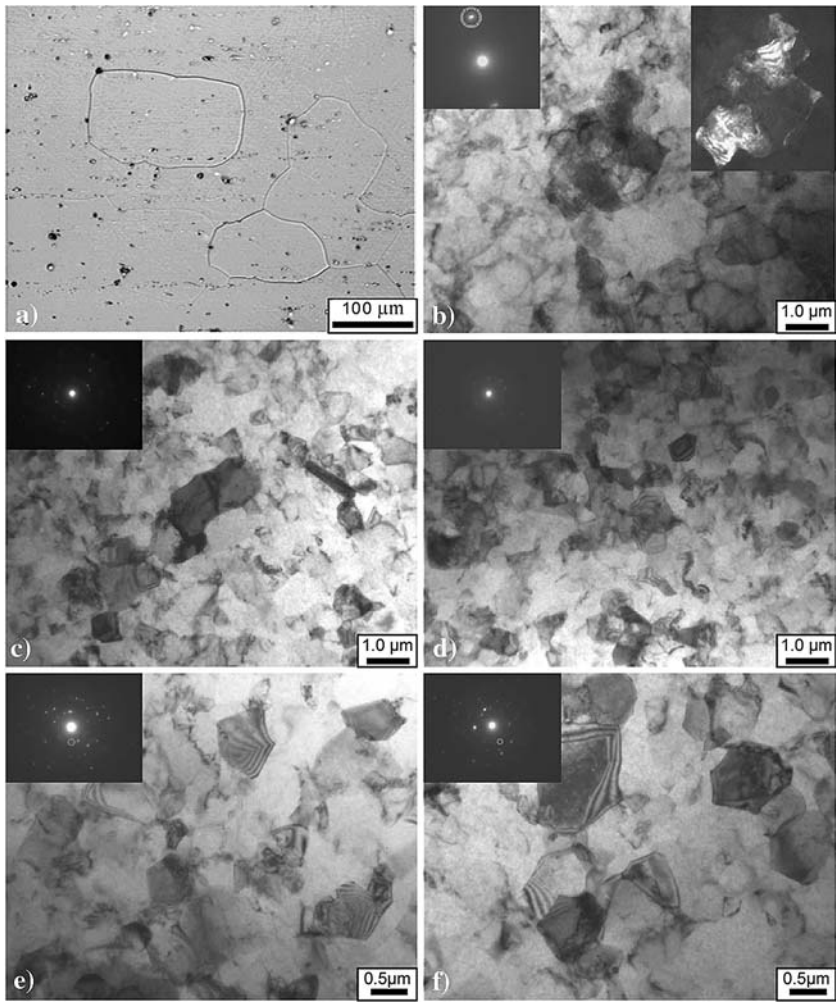

Fig. 7 Microstructures of aluminium: (**a**) optical microscopy showing the initial annealed structure and TEM showing the structure after applying a pressure of $P = 1$ GPa: (**b**) without torsional straining; after 2 whole revolutions (**c**) in the central region and (**d**) near the periphery; after 8 whole revolutions (**e**) in the central region and (**f**) near the periphery

~ 1 μm and it is further reduced to ~0.8 μm after 8 whole revolutions. No visible difference can be found in the microstructures in the centre and in the periphery in HPT samples after 2 revolutions. Increasing straining (up to 8 whole revolution) leads to a slight decrease of the mean grain size and there appears to be a slightly smaller grain size in the central region of the disk. This suggests that recovery processes may have begun in the highly-strained region at the periphery.

Microtexture and grain boundary statistics in HPT nickel and aluminium

The detailed results for an OIM study of HPT nickel were reported earlier [23]. Now the data are re-analysed using an identical clean-up procedure for the OIM nickel and aluminium raw data as described in Section 3.

Figure 8 shows an IPF map of CP aluminium subjected to pure compression without any torsional straining. The primary grain boundaries (thick lines) and developed substructure (thin lines) are readily apparent. The discrete inverse pole figure (Fig. 8b) shows a concentration near the 110 pole in consistency with data reported in the literature [34]. Figure 9 depicts IPF colour maps from the centre and periphery for HPT aluminium disks for 2 whole revolutions (Fig. 9 a, b) and for 8 whole revolutions (Fig. 9 c, d). On the right side are shown discrete pole figures plotted on the flow plane. The OIM microstructures are satisfactorily similar for the central region and periphery for specimen after 2 and 8 whole revolutions. The pole figures indicate a simple shear texture which is stronger for the central region and scattered for the periphery in the case of the specimen after 8 revolutions. This indicates that recrystallization takes place.

Figure 10 depicts three-dimensional ODF for HPT nickel ($P = 6$ GPa, $N = 5$) and CP aluminium ($P = 1$ GPa, $N = 8$) taken from the periphery. Both ODF possess the main components of a shear texture. The CP aluminium ODF has pipes at $\Phi = 0$ which correspond to a (100) cube texture.

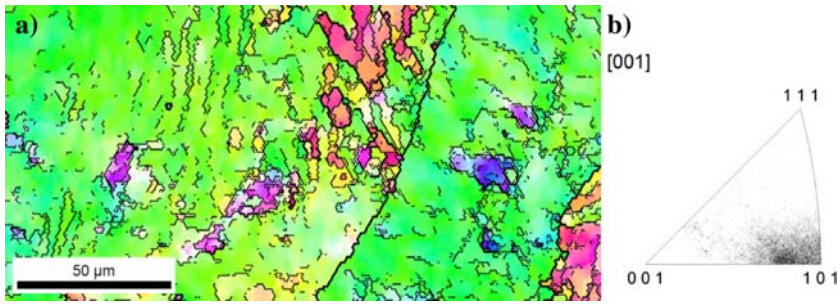

Fig. 8 (**a**) OIM structure of HPT aluminium after applying a pressure of $P = 1$ GPa without torsional sraining; (**b**) corresponding to the inverse pole figure recorded in the shear plane

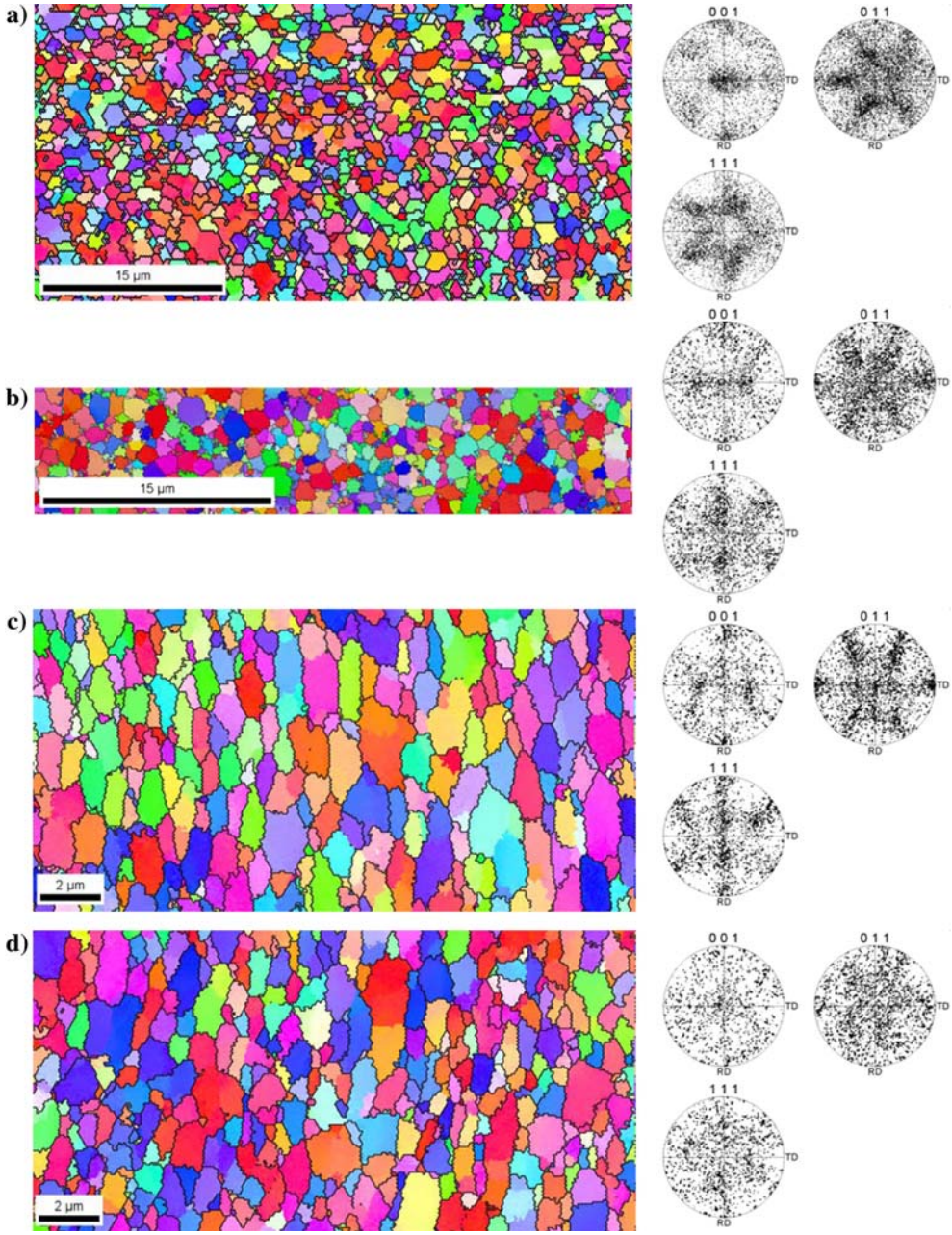

Fig. 9 OIM structure of HPT aluminium after applying a pressure of $P = 1$ GPa: after 2 whole revoutions: (**a**) in the central region (**b**) near the periphery; after 8 whole revoutions: (**c**) in the central region (**d**) near the periphery

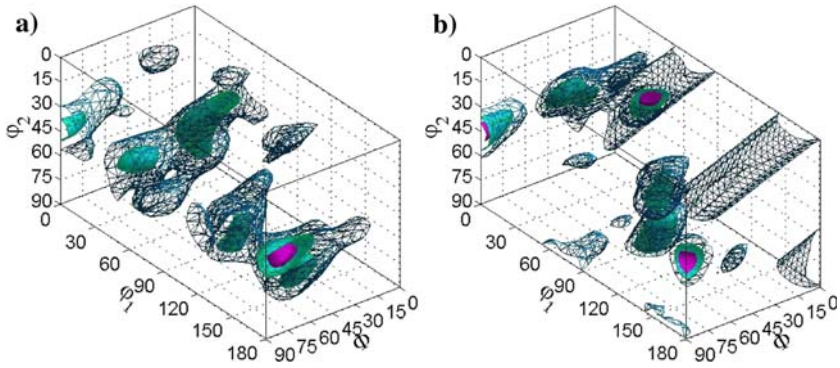

Fig. 10 Three-dimensional ODF plottted on the flow plane of the HPT disk of (**a**) nickel (P = 6 GPa, N = 5) and (**b**) CP aluminium (P = 1 GPa, N = 8). Data were recorded near the periphery of the disks

The grain boundary (GB) statistics were measured for a statistically significant number of grains (more than 500 grains) from the edge and the centre of the HPT sample, respectively. These GB statistics are presented both in terms of the GB character distributions as measured by the misorientation angles and by the reciprocal density of coincidence sites where four distinct sets of boundaries were defined: low-angle boundaries (Σ1), twins or Σ3 boundaries, and high-angle random grain boundaries. Following conventional practice, the various types of GB were classified according to CSL-theory using the nearness (or Brandon) condition of $\Delta\theta = 15^\circ \cdot \Sigma^{-1/2}$ [35] with all low-angle boundaries designated as Σ1 boundaries and having misorientations up to a maximum of 15°.

Figure 11 shows grain boundary misorientation distributions (GBMD) for HPT nickel (Fig. 11 a) and CP aluminium after 2 (Fig. 11b) and 8 (Fig. 11c) whole revolutions. The left-hand column represents GBMD of the central region and the right-hand column shows grain boundary statistics from the periphery. The central region shows a higher fraction of low angle boundaries for all specimens. The HPT aluminium specimens (even after 8 whole revolutions) possess in general a higher fraction of LAB comparing to HPT nickel. Table 1 represents the grain boundary character distribution (GBCD) for HPT nickel and aluminium disks in terms of the fraction of LAB, twins (Σ3) and high-angle boundaries. As described in Section 3, the clean-up procedure used in the present paper has slightly changed the GBCD for nickel compared to the earlier report [23]. Nevertheless, all distributions have significant fractions of high-angle boundaries.

Discussion

This investigation leads to two important conclusions regarding the processing of samples by HPT. First, HPT is extremely effective in producing an exceptionally small grain size in bulk metals: in pure Ni the present experiments give an average grain size of ~170 nm under optimum processing conditions and in CP aluminium there is a mean grain size of ~1 μm. Further refinement in HPT aluminium is limited by recrystalizaion due to the high homologous temperature of HPT processing (T/T_M ~ 0.4–0.5) compared to nickel (T/T_M ~ 0.2–0.3). Second, the results provide very clear evidence that a reasonably homogeneous microstructure may be formed throughout the sample using HPT processing provided the applied pressure is high and the sample is torsionally strained through a sufficiently large number of revolutions. In these experiments, a homogeneous microstructure was achieved in pure Ni at both the centre and the periphery of the sample, together with identical grain boundary statistics as shown in Fig. 11 and Table 1, after HPT processing through a significant number of whole revolutions under high applied pressure. Furthermore, from quantitative measurements of the grain boundary statistics, it is demonstrated that these experimental conditions give not only a smaller grain size but also there is a significantly lower fraction of low-angle boundaries in HPT (~20%) compared to other SPD processes (for example, in the same material when processed by ECAP where the fraction of low-angle boundaries is ~27% [6]).

The detailed microhardness measurements documented in Figs. 4 and 5 lead to the conclusion that deformation develops in HPT in an essentially undulating manner and these observations therefore provide an opportunity to propose a simple mechanism to explain the development of a homogeneous microstructure during large-scale deformation in HPT processing.

It is reasonable to assume that shear takes place initially in a place where the friction coefficient is high and therefore at a point that is dependent both upon the local surface roughness of the disk and/or the anvil and upon the applied pressure. However, it is also

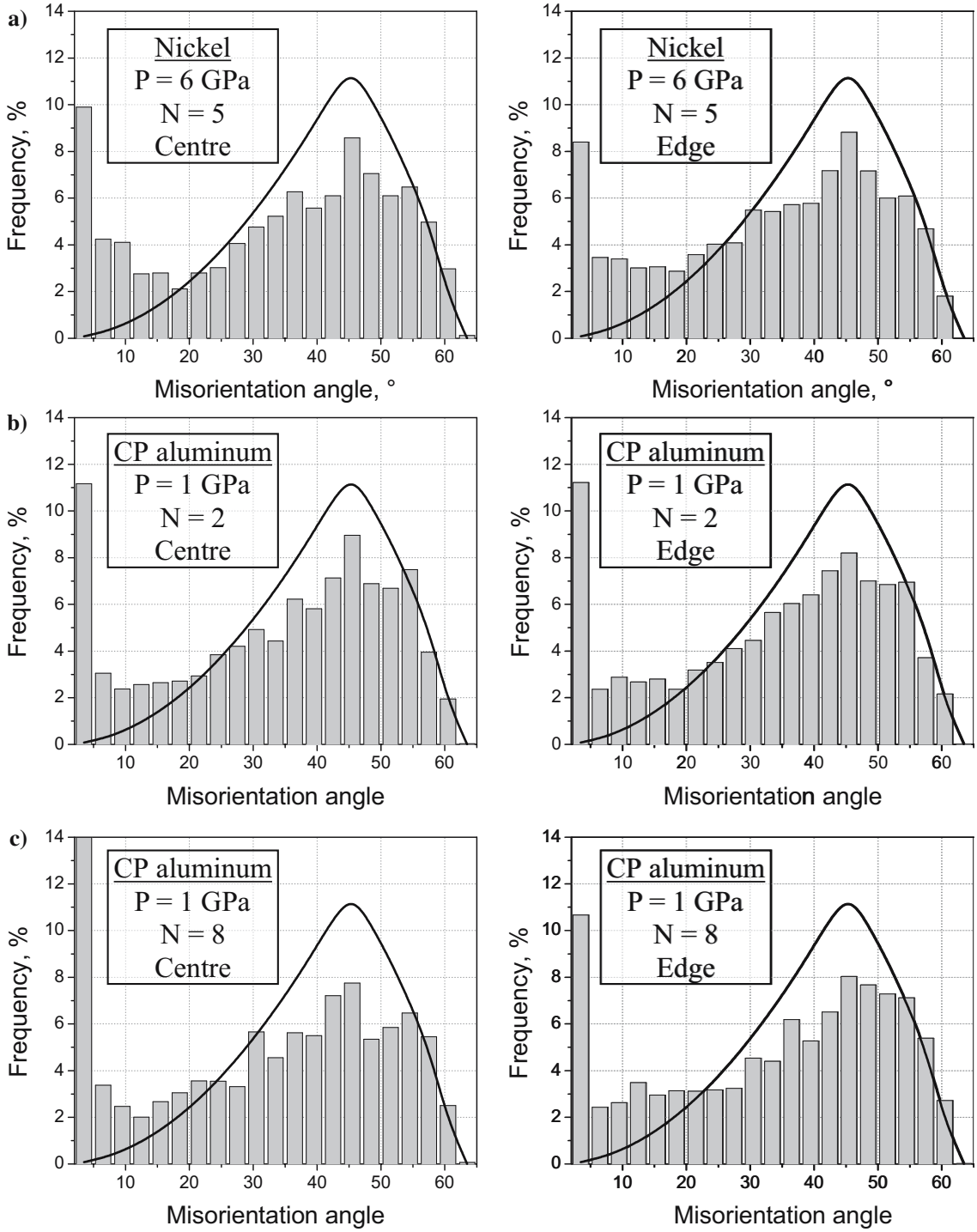

Fig. 11 Grain boundary misorientation distributions in HPT (**a**) nickel (P = 6 GPa, N = 5), (**b**) CP aluminium (P = 1 GPa, N = 2) and (**c**) CP aluminium (P = 1 GPa, N = 8). Left column corresponds to the central region, right column corresponds to the periphery

apparent that the occurrence of shearing will introduce local hardening at this particular point and this gives a consequent reduction in the frictional forces so that the shearing is then transferred to an adjacent position. In practice, this leads to the development of deformation in a repetitive manner throughout the outer ring of the disk and thereafter the shearing will extend to the interior.

A repetitive process of this type can explain the undulations visible in the three-dimensional hardness

Table 1 Grain boundaries statistics in fcc metals subjected to HPT

GBs type	Nickel, P = 6 GPa, N = 5		Aluminium, P = 1 GPa, N = 0		Aluminium, P = 1 GPa, N = 2		Aluminium, P = 1 GPa, N = 8	
	Centre	Periphery	Centre	Periphery	Centre	Periphery	Centre	Periphery
LAB	22.0	19.3	93.5	80.2	23.0	20.3	20.0	20.0
Σ3	2.6	2.3	0.0	0.3	2.3	1.7	1.8	1.7
HAB	75.4	78.4	6.5	19.5	74.7	78.0	78.2	78.3

meshes shown in Figs. 4 and 5 and the mechanism is supported by the undulations which are evident in the local distributions of the microhardness values. For example, the presence of these undulations may be demonstrated by plotting, in arbitrary units, the average curvature of the microhardness measurements across the diameter of the disk as a function of the number of whole revolutions.

The results from these observations show that, in terms of the microhardness measurements and the TEM and OIM observations, the microstructure of fcc pure metals becomes reasonably homogeneous after an optimal number of whole revolutions of HPT using either an unconstrained or a constrained HPT facility. The results support earlier observations on pure Ni, an Al alloy and a NiTi alloy [28] but they are not consistent with microhardness data reported recently when processing an austenitic steel using HPT [24]. One explanation may be a non-coaxial alignment of the HPT anvil for the unconstrained condition [24]. In fact, partial support for this suggestion is found by careful inspection of Figs. 4 and 5 where the minimum Hv points are not precisely in the geometric centre of the nickel disk processed by unconstrained HPT. However, the constrained HPT experiments adopted for CP aluminium also support the conclusion that the optimal conditions used for HPT processing lead to a sufficiently homogenous microstructure across the disk. Thus, an alternative explanation may lie in the greater difficulty in reaching homogeneity in a material, such as steel, where the microstructure is complex. Recently, a deformation-induced martensitic transformation was observed in an austenitic steel [36] and accordingly it is reasonable to assume that some plastic energy is used for this transformation process. This suggests, therefore, that there may be insufficient energy in the central regions of disks of austenitic steel to effectively refine the microstructure.

Conclusions

Experiments were conducted to investigate the microstructural evolution in pure nickel and commercial purity aluminium during HPT processing using constrained and unconstrained processing conditions.

Processing by high-pressure torsion (HPT) produces a significant increase in hardness and a very substantial grain refinement in bulk metals: in the present experiments on pure Ni, the hardness was increased from ~1.4 GPa to > 3 GPa and the grain size was reduced from ~100 μm to ~170 nm.

Using the three separate procedures of microhardness measurements, transmission electron microscopy and orientation imaging microscopy, it is shown that HPT may be used effectively to develop an essentially homogeneous microstructure throughout the sample provided the applied pressure and the torsional strain (as measured in terms of the number of revolutions) are sufficiently high. From quantitative measurements using orientation imaging microscopy, it is shown that the homogeneous microstructures produced by HPT contain larger fractions of low-angle, twin and special boundaries but a smaller fraction of high-angle random boundaries than anticipated in a random distribution. However, the distributions of misorientation angles in these homogeneous microstructures are essentially identical in the centre and at the periphery of the deformed disks.

Acknowledgements This work was partially supported by INTAS-03513779 and RFBR-05-03-32233-a. One of the authors (APZ) thanks the National Research Council of the National Academy of Science (USA) and the Spanish Ministry of Education and Science (under Ramón y Cajal program) for financial support. The other authors were partially supported by the U.S. Air Force Office of Scientific Research under funding document no. F1ATA06058G001 (TRM) and the National Science Foundation of the United States under Grant No. DMR-0243331 (TGL).

References

1. Segal VM, Reznikov VI, Drobyshevskiy AE, Kopylov VI (1981) Russ Metall 1:99
2. Smirnova NA, Levit VI, Pilyugin VI, Kuznetsov RI, Davydova LS, Sazonova VA (1986) Fiz Metal Metalloved 61:170
3. Horita Z, Smith DJ, Furukawa M, Nemoto M, Valiev RZ, Langdon TG (1996) J Mater Res 11:1880
4. Iwahashi Y, Horita Z, Nemoto M, Langdon TG (1998) Metall Mater Trans 29A:2503

5. Stolyarov V, Valiev RZ (2002) In: Zhu YT, Langdon TG, Mishra RS, Semiatin SL, Saran MJ, Lowe TC (eds) Ultrafine grained materials II. The Minerals, Metals and Materials Society, Warrendale, PA, p 209
6. Zhilyaev AP, Kim B-K, Nurislamova GV, Baró MD, Szpunar JA, Langdon TG (2002) Scripta Mater 48:575
7. Stolyarov VV, Zhu YT, Lowe TC, Islamgaliev RK, Valiev RZ (1999) Nanostruct Mater 11:947
8. Mishra RS, Valiev RZ, McFadden SX, Islamgaliev RK, Mukherjee AK (2001) Phil Mag A 81:37
9. Islamgaliev RK, Yunusova NF, Sabirov IN, Sergueeva AV, Valiev RZ (2001) Mater Sci Eng A319–322:877
10. Dobatkin SV (2002) In: Zhu YT, Langdon TG, Mishra RS, Semiatin SL, Saran MJ, Lowe TC (eds) Ultrafine grained materials II. The Minerals, Metals and Materials Society, Warrendale, PA, p 183
11. Islamgaliev RK, Buchgraber W, Kolobov YR, Amirkhanov NM, Sergueeva AV, Ivanov KV, Grabovetskaya GP (2001) Mater Sci Eng A319–321:872
12. Oh-ishi K, Horita Z, Smith DJ, Valiev RZ, Nemoto M, Langdon TG (1999) J Mater Res 14:4200
13. Dudova N, Kaibyshev R, Valitov V (2002) In: Zhu YT, Langdon TG, Mishra RS, Semiatin SL, Saran MJ, Lowe TC (eds) Ultrafine grained materials II. The Minerals, Metals and Materials Society, Warrendale, PA, p 75
14. Korznikov AV, Dimitrov O, Korznikova GF, Dallas JP, Idrisova SR, Valiev RZ, Faudet F (1999) Acta Mater 47:3301
15. Korznikov AV, Tram G, Dimitrov O, Korznikova GF, Idrisova SR, Pakiela Z (2001) Acta Mater 49:663
16. Valiev RZ, Song C, McFadden SX, Mukherjee AK, Mishra RS (2001) Phil Mag A 81:25
17. Mishra RS, Stolyarov VV, Echer C, Valiev RZ, Mukherjee AK (2001) Mater Sci Eng A298:44
18. Korznikov AV, Ivanisenko YuV, Laptionok DV, Safarov IM, Pilyugin VP, Valiev RZ (1994) Nanostruct Mater 4:159
19. Dobatkin SV, Valiev RZ, Kaputkina LM, Krasilnikov NA, Sukhostavskaya OV, Komlev VS (1999) In: Sakai T, Suzuki HG (eds) The Fourth International Conference on Recrystallization and Related Phenomena. The Japan Institute of Metals, Sendai, Japan, p 907
20. Dobatkin SV, Valiev RZ, Odessky PD, Krasilnikov NA, Raab GI, Konenkova VN (2001) In: Takaki S, Maki T (eds) Ultrafine-grained steels. The Iron and Steel Institute of Japan, Tokyo, Japan, p 122
21. Kaibyshev R, Kazakulov I, Sakai T, Belyakov A (2001) In: Takaki S, Maki T (eds) Ultrafine-grained steels. The Iron and Steel Institute of Japan, Tokyo, Japan, p 152
22. Ivanisenko YuV, Valiev RZ, Lojkowski W, Grob A, Fecht H-J (2002) In: Zhu YT, Langdon TG, Mishra RS, Semiatin SL, Saran MJ, Lowe TC (eds) Ultrafine grained materials II. The Minerals, Metals and Materials Society, Warrendale, PA, p 47
23. Zhilyaev AP, Nurislamova GV, Kim B-K, Baró MD, Szpunar JA, Langdon TG (2003) Acta Mater 51:753
24. Vorhauer A, Pippan R (2004) Scripta Mater 51:921
25. Sakai G, Horita Z, Langdon TG (2005) Mater Sci Eng A393:344
26. Zhilyaev AP, Oh-ishi K, Langdon TG, McNelley TR (2006) In: Zhu YT, Langdon TG, Horita Z, Zehetbauer MJ, Semiatin SL, Lowe TC (eds) Ultrafine grained materials IV. The Minerals, Metals & Materials Society, Warrendale, PA, p 245
27. Zhilyaev AP, Oh-ishi K, Langdon TG, McNelley TR (2006) In: Zhu YT, Langdon TG, Horita Z, Zehetbauer MJ, Semiatin SL, Lowe TC (eds) Ultrafine grained materials IV. TMS, Warrendale, PA, p 245
28. Prokoshkin SD, Khmelevskaya IYu, Dobatkin SV, Trubitsyna IB, Tatyanin EV, Stolyarov VV, Prokofiev EA (2005) Acta Mater 53:2703
29. Zhilyaev AP, Kim B-K, Szpunar JA, Baró MD, Langdon TG (2005) Mater Sci Eng A391:377
30. Polakowski NH, Ripling EJ (1966) ''Strength and structure of engineering materials'', Prentice-Hall, Englewood Cliffs, NJ
31. Degtyarev MV, Chashchukhina TI, Voronova LM, Davydova LS, Pilyugin VP (2000) Phys Metals Metallog 90:604
32. Efros BM, Pilyugin VP, Patselov AM, Beygelzimer YY, Efros NB (2002) In: Zhu YT, Langdon TG, Mishra RS, Semiatin SL, Saran MJ, Lowe TC (eds) Ultrafine grained materials II. The Minerals, Metals and Materials Society, Warrendale, PA, p 193
33. Dingley DJ, Field DP (1996) Mater Sci Technol 12:1
34. Stout MG, Kallend JS, Kocks UF, Przystupa MA, Rollett AD (1988) In: Kallend JS, Gottstein G (eds) Eighth International Conference on Texture of Materials. The Metallurgical Society, Warrendale, PA, p 479
35. Brandon DG (1966) Acta Metall 14:1479
36. Rybal'chenko OV, Dobatkin SV, Kaputkina LM, Raab GI, Krasilnikov NA (2004) Mater Sci Eng A387–389:244